ARTICLE

Advantages to a diverging Raman amplifier

James D. Sadler [1], Luís O. Silva [2], Ricardo A. Fonseca [2], Kevin Glize[3], Muhammad F. Kasim[1], Alex Savin [1], Ramy Aboushelbaya[1], Marko W. Mayr [1], Benjamin Spiers [1], Robin H.W. Wang[1], Robert Bingham[3,4], Raoul M.G.M. Trines[3] & Peter A. Norreys[1,3]

The plasma Raman instability can efficiently compress a nanosecond long high-power laser pulse to sub-picosecond duration. Although, many authors envisaged a converging beam geometry for Raman amplification, here we propose the exact opposite geometry; the amplification should start at the intense focus of the seed. We generalise the coupled laser envelope equations to include this non-collimated case. The new geometry completely eradicates the usual trailing secondary peaks of the output pulse, which typically lower the efficiency by half. It also reduces, by orders of magnitude, the initial seed pulse energy required for efficient operation. As in the collimated case, the evolution is self similar, although the temporal pulse envelope is different. A two-dimensional particle-in-cell simulation demonstrates efficient amplification of a diverging seed with only 0.3 mJ energy. The pulse has no secondary peaks and almost constant intensity as it amplifies and diverges.

[1] Clarendon Laboratory, University of Oxford, Parks Road, Oxford OX1 3PU, UK. [2] GoLP/Instituto de Plasmas e Fusão Nuclear, Instituto Superior Tecnico, Universidade de Lisboa, Lisbon 1049-001, Portugal. [3] Central Laser Facility, STFC Rutherford Appleton Laboratory, Didcot OX11 0QX, UK. [4] Department of Physics, University of Strathclyde, 107 Rottenrow East, Glasgow G4 0NG, UK. Correspondence and requests for materials should be addressed to J.D.S. (email: james.sadler@physics.ox.ac.uk)

The method of chirped pulse amplification has massively increased the peak power of laser pulses. Modern lasers can reach intensities exceeding 10^{21} W cm^{-2}, high enough that the free electrons undergo relativistic oscillations in the wave. This high intensity is achieved by compressing the pulses to their transform limited duration with a set of reflective gratings, and subsequent focussing[1]. However, the damage threshold of these components limits the peak achievable intensity.

There are predictions that even greater intensities, of the order 10^{24} W cm^{-2}, will introduce quantum electro-dynamics processes, such as vacuum phase shifts[2,3] and electron–positron pair production[4]. The resultant gamma ray bursts will have numerous applications in nuclear physics[5] and industrial sensing. However, it is impractical and expensive to scale up current solid-state optics, and so laser compressors with greater damage thresholds may be required to study these processes. High energy picosecond pulses, ideally in the ultra-violet, also have implications in inertial confinement fusion. The fast particle beams generated by these short pulses would provide auxiliary heating to the fusion fuel, either through collisional stopping[6,7] or two beam instabilities[8–10]. Since damage thresholds of solid state devices decrease in the ultra-violet range, ionised compression or gain media will be required.

It was discovered by Malkin et al.[11] that a plasma can act as a pulse compressor, with an electron plasma wave mediating energy from one pulse to another. This proceeds so long as the short seed pulse has frequency $\omega_1 = \omega_0 - \omega_p$, where ω_0 is the frequency of the counter-propagating long-pump pulse and ω_p is the electron plasma frequency[12]. Plasma permits a much higher output intensity than solid state optics[13], possibly by a factor of 10^5. The plasma should be uniform[14] and approximately one hundredth of the pump pulse critical density[15,16].

In the original proposal for Raman amplifiers, a pre-focussed geometry was envisaged[11]. However, in the derivation given there, the beams were assumed to be collimated. In this work, we generalise those coupled envelope equations to include the case of a converging or diverging Gaussian beam and recover the results of Malkin et al.[11] as a special case. We show that the new diverging geometry minimises the required seed pulse energy. It also eliminates the wastage of energy in to the usual trailing secondary peaks of the amplified pulse. These facts indicate that a greater output power will be achievable using the diverging geometry, rather than a collimated geometry.

Results

Proposed geometry. The collimated amplifier evolves as follows[17]: energy is transferred from the pump to the seed pulse, and in the non-linear stage of the instability, the pump is fully depleted. The seed pulse amplitude a_1 grows linearly with time. The pump and seed amplitudes are defined as $a_{0,1} = eE_{0,1}/(m\omega_{0,1}c)$, where m is the electron mass, E_0 is the peak electric field of the pump and E_1 is that of the seed. As it amplifies, the full width at half maximum duration of the seed pulse T_1 decreases inversely proportional to time, such that

$$a_1 T_1 \sqrt{\omega_0 \omega_p} \simeq 5. \qquad (1)$$

In fact, Eq. (1) also gives the condition for the Raman scatter to deplete the pump pulse[15]. Since the energy transfer is proportional to the pump depletion, the amplification is only highly efficient when Eq. (1) is met.

However, this requirement on a_1 poses a problem, since it is difficult to generate intense seed pulses at the shifted wavelength. One method is to utilise non-linear optics effects in a neutral gas cell. It may also be possible to use optical parametric chirped pulse amplification to generate intense tune-able seed pulses, at the cost of increased complexity and timing issues. Even in the most successful experiment yet[18,19], the 880 nm wavelength seed pulse only had $a_1 T_1 \sqrt{\omega_0 \omega_p} \simeq 0.3$. The measured plasma amplifier energy efficiency was 6.4%. The low power seed meant this was far below the theoretical maximum of $1 - \omega_p/\omega_0 \simeq 90\%$.

Since Eq. (1) is independent of the transverse dimension, an obvious tactic to reach the non-linear stage is to start the amplification with the seed pulse at its focus, where its intensity is maximum. This is in contrast to the geometry proposed in ref.[11]. For example, a 1 μm wavelength, 50 fs seed pulse with energy 1 mJ in a plasma of electron density 10^{19} cm^{-3} could easily achieve $a_1 T_1 \sqrt{\omega_0 \omega_p} = 5$ with a focal beam waist of 6 μm. In addition, this high initial seed intensity will also permit use of the seed ionisation scheme[20–22], where the plasma is not ionised until the short seed pulse arrives. This has the significant advantages of keeping the electron temperature low and avoiding instabilities of the pump pulse, since it traverses a neutral gas until it meets the seed.

With such a narrow beam waist, the amplifier length may be longer than the Rayleigh length and so it is not valid to assume a collimated beam. In fact, we will now assume that the amplification occurs outside of the Rayleigh range. The new proposed geometry is shown in Fig. 1. The seed approaches from the left side and is amplified as it diverges through the plasma. Note that this closely replicates the geometry of typical high-power laser systems, which start with a low power, narrow seed and increase the diameter as it amplifies. The pump and seed overlap may be maximised by matching the focal geometry of the pump to that of the seed, with the pump counter-propagating.

The disadvantage of this scheme is that the amplified pulse will require subsequent focussing. However, it may exceed the damage threshold of conventional optics. It should be possible to focus it with a spherical plasma mirror[23,24], as shown in Fig. 1. This will have the added advantage of improving the pulse contrast. The mirror may be placed at a position where the low intensity pump will propagate through the back of it, but the amplified pulse will ionise and reflect from it. Alternatively, the pump may arrive from a different angle, past the side of the plasma mirror. This mirror will allow control over the final focal position.

The transverse beam profile outside of the Rayleigh range may be a concern, however the low energy of the seed pulse will allow the use of adaptive optics to smooth any transverse phase imperfections. As shown in ref.[25], the pump pulse must be energetic, but need not have the same coherence, since any
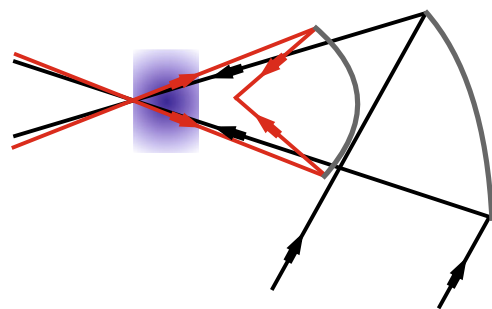

Fig. 1 Schematic of the proposed diverging Raman amplifier geometry. The seed pulse (red) starts in the amplifier at its focus, where it is met by the counter-propagating long-pump pulse (black). It amplifies through the plasma (purple) as it diverges outside of the Rayleigh range. A curved plasma mirror (grey) focusses the amplified pulse to a controllable focal position. Alternatively, the pump may arrive from a different angle, past the side of the plasma mirror

imperfections will be transferred to the plasma wave and not the amplified pulse. A longer amplifier for the compression of nanosecond pulses will also use a much lower plasma density[26], lowering the effect of competing instabilities.

Generalisation of the envelope equations. To investigate how the beam geometry affects the amplification, the coupled envelope equations from ref.[11] will now be generalised to include non-collimated beams. Including the transverse diffraction term from the paraxial Helmholtz equation, the amplified pulse amplitude $a_1(x, t)$ evolves as[27]

$$\partial_t a_1 - c\partial_x a_1 - \frac{ic^2}{2\omega_1}\left(\partial_y^2 + \partial_z^2\right)a_1 = -\frac{\omega_p^2}{4\omega_1}a_0 n_2^*. \quad (2)$$

In this equation, spatial and temporal partial derivatives are written as ∂_x and ∂_t. The pulse propagates along the x axis and the origin is at the focus. The dimensionless plasma wave amplitude n_2 is normalised to the average electron density. The dispersion of the waves is neglected. The amplified pulse vector potential is given by the real part of $\hat{y}(mc/e)a_1 \exp(ik_1 x + i\omega_1 t)$. The envelope model assumes that the pulses are much longer than one wavelength and damping processes are negligible.

To maximise the pulse overlap, the length of the amplifier should be $cT_0/2$, where T_0 is the pump pulse duration. For a 1 ns long-pump pulse, as found at many high-power laser facilities, the amplifier will be 15 cm long. For the parameters described earlier, the beam waist was $w_f = 6 \,\mu\text{m}$, giving the Rayleigh length $L_R = \omega_1 w_f^2/(2c) = 113 \,\mu\text{m}$. This means most of the amplification length will have $x \gg L_R$.

Assuming the seed pulse is a perfect Gaussian beam along the x axis, the transverse Laplacian can be evaluated to give the amplitude on the x axis as

$$\partial_t a_1 - c\partial_x a_1 + \frac{icL_R}{x^2}a_1 - \frac{c}{x}a_1 = -\frac{\omega_p^2}{4\omega_1}a_0 n_2^*. \quad (3)$$

The third and fourth terms have been Taylor expanded to leading order, assuming that $x \gg L_R$. This assumption also means the third term in Eq. (3) is negligible with respect to the fourth. Furthermore, the maximum of the short pulse will be close to the position $x = -c(t - t_f)$, where t_f is the time of best focus. This is the approximate coordinate for the whole pulse, assuming that the pulse duration is much less than $t - t_f$. The seed pulse propagates towards negative x and the pump pulse propagates towards positive x. In typical situations, the plasma is very under-dense, so that $\omega_p \ll \omega_0$. Along with the other equations from ref. [11], this leads to the system

$$(\partial_t + 2c\partial_x)a_0 = \frac{\omega_p^2}{4\omega_0}a_1 n_2, \quad (4)$$

$$\partial_t a_1 + \frac{a_1}{t - t_f} = -\frac{\omega_p^2}{4\omega_1}a_0 n_2^*, \quad (5)$$

$$(\partial_t + c\partial_x)n_2 = -\frac{\omega_0^2}{\omega_p}a_0 a_1^*. \quad (6)$$

The time t is measured from the start of the non-linear stage. The equations have been written in a spatial coordinate system moving along with the seed pulse, with the front of the seed pulse remaining approximately at $x = 0$. The new geometric term has

been neglected for the plasma wave, since its phase velocity is much less than c. In addition, the unperturbed pump amplitude will barely change within the extent of the short seed pulse, so its geometrical term can be neglected. However, since the pump is focussing and its power may change, the incoming pump amplitude $a_0(t, 0)$ is treated as time dependent.

Following the method of ref.[11], when the pump is heavily depleted, the interaction will be short and so the time derivatives may be neglected with respect to the spatial derivatives in Eqs. (4) and (6). This will give the evolution in the late non-linear stage, where the seed duration is much less than its timescale of evolution. The equations become

$$2c\partial_x a_0 = \frac{\omega_p^2}{4\omega_0}a_1 n_2, \quad (7)$$

$$\partial_t a_1 + \frac{a_1}{t - t_f} = -\frac{\omega_p^2}{4\omega_1}a_0 n_2^*, \quad (8)$$

$$c\partial_x n_2 = -\frac{\omega_0^2}{\omega_p}a_0 a_1^*. \quad (9)$$

Again following refs. [11, 20], we now introduce the trial function $u(x, t)$ and the trial solutions $a_0(x, t) = \alpha_0(t) \cos(u/2)$, $a_1(x, t) = \alpha_1 c\partial_x u$ and $n_2(x, t) = \alpha_2(t)\sin(u/2)$. The variable α_0 is the incoming pump amplitude at the start of the seed pulse.

Substituting these trial solutions in to Eqs. (7) and (9) leads to $\alpha_1 = \sqrt{2/\left(\omega_0\omega_p\right)}$ and $\alpha_2 = -\alpha_0(2\omega_0/\omega_p)^{3/2}$. Equation (8) then gives

$$\left(\partial_t + \frac{1}{t - t_f}\right)\partial_x u = \frac{\omega_0\omega_p}{4c}\alpha_0^2 \sin(u). \quad (10)$$

Self-similar amplification. We first find the solution for constant pump pulse amplitude, when α_0 is constant. In this case there is a self-similar solution[11]. This means that the amplitudes of the three waves, for all values of x and t, depend only on the dimensionless coordinate $\beta = \omega_0\omega_p\alpha_0^2 xt/(4c)$. This can be shown by changing variables in Eq. (10) and writing $u(x, t) = f(\beta)$, leading to

$$\beta\frac{d^2 f}{d\beta^2} + \left(\frac{2t - t_f}{t - t_f}\right)\frac{df}{d\beta} = \sin(f). \quad (11)$$

The variable t has not been eliminated by the change of variables and so the evolution of the pulse is not, in general, self similar. However, in the limit $|t_f| \gg t$, Eq. (11) depends only on β and the equation reduces to the self-similar behaviour found in ref. [11]. In this limit, the focus is very far away compared to the scale of the interaction.

There is also self-similar behaviour in the limit $|t_f| \ll t$, which applies when the non-linear stage starts at or very near the focus of the amplified pulse. Since t is positive, this means $t - t_f > 0$ and so this limit will only apply to the case of a diverging beam and not a converging beam. This is the limit illustrated in Fig. 1. In this new geometry, the self similar equation becomes

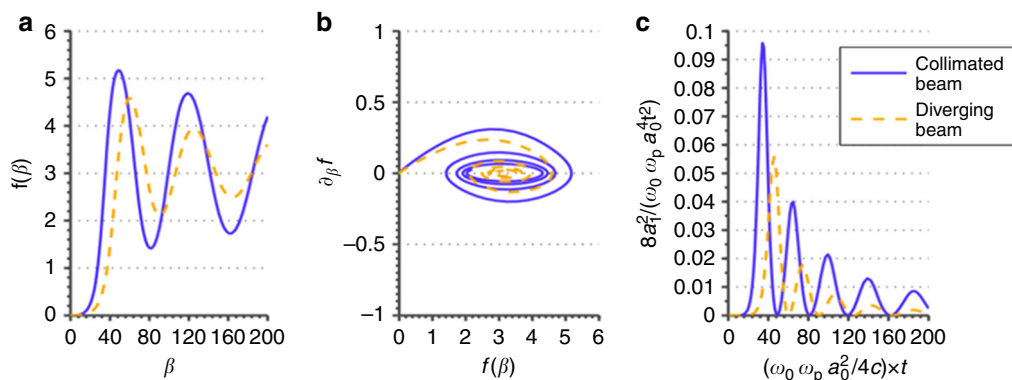$$\beta\frac{d^2 f}{d\beta^2} + 2\frac{df}{d\beta} = \sin(f). \quad (12)$$

Fig. 2 Numerical integration of the self-similar equations for the limit of a collimated beam (solid line) or a diverging beam (Eq. (12), dashed line). The boundary condition was $f(0) = 0$ and $f'(0) = 0.001$, corresponding to a small initial seed. **a** f as a function of the dimensionless self-similar coordinate β. It tends towards π for both cases. **b** The development in the f, f' plane. **c** The shape of the amplified pulse temporal power envelope, as found from these solutions. Propagation is towards the left

This equation is identical to that of the collimated case with $|t_f| \gg t$, found by Malkin et al.[11], except the coefficient of the first order term is increased from 1 to 2.

The numerical solution to Eq. (12) is shown in Fig. 2. It has a similar form to the standard collimated solution. The pulse is composed of many peaks that are slightly lower intensity than in the collimated case, although a greater fraction of the energy now resides in the main front-most peak. The Eq. (1) still holds. The usual scaling laws still hold, so that the pulse amplitude increases $a_1 \propto t$ and the seed duration shortens $\propto 1/t$. Considering the divergence of the pulse, the seed power increases $\propto t^4$ and the seed energy increases $\propto t^3$.

Steady-state amplification. Returning to Eq. (10), there is a solution when $\partial_t u = 0$. The steady-state solution satisfies

$$\partial_x u = \frac{\omega_0 \omega_p (t - t_f)}{4c} \alpha_0^2 \sin(u). \tag{13}$$

Therefore, if $\alpha_0 \propto 1/\sqrt{t - t_f}$ then the amplified pulse will have a temporal envelope that is constant as it amplifies. The pulse intensity and duration will be constant, however the power and energy will increase $\propto t^2$ as the pulse diverges.

For the converging pump pulse in three dimensions, $\alpha_0 \propto 1/\sqrt{t - t_f}$ requires its power to increase linearly with time $\propto t - t_f$. Pulse shaping such as this is routinely achieved on many large-scale systems such as the national ignition facility[28]. Introducing the proportionality constant $a = (t - t_f) \alpha_0^2 \sqrt{\omega_0 \omega_p / 8}$, the solution to Eq. (13) is

$$\tan\left(\frac{u}{2}\right) = \exp\left(a \sqrt{\frac{\omega_0 \omega_p}{2c^2}}(x - x_0)\right) \tag{14}$$

$$a_1(x) = a \, \text{sech}\left(a \sqrt{\frac{\omega_0 \omega_p}{2c^2}}(x - x_0)\right). \tag{15}$$

The constant a is therefore the peak amplitude of the scattered pulse. The integration constant x_0 is the position of the pulse maximum.

After an initial start-up stage, the pulse converges towards a single, constant intensity spike that monotonically depletes the pump pulse. There are no trailing secondary peaks. This has great

significance, since in the collimated case as much as 40% of the pulse energy is wasted in to the secondary peaks, shown by the solid line in Fig. 2c. The increased prominence of the first spike of the amplified pulse is comparable to that predicted by Toroker et al.[29] when a chirped seed pulse is used. For the steady-state amplifier, the amplitude duration product is modified to

$$a T_1 \sqrt{\omega_0 \omega_p} \simeq 2.5. \tag{16}$$

Equations (1) and (16) show that, for the same energy, the diverging pulse will have four times the peak power of a pulse from a collimated amplifier.

Taken together, these facts mean that a much greater peak intensity could be reached with the diverging beam scheme rather than the collimated scheme, possibly by a factor of four or more. A shorter, single spike is the desired pulse profile for many uses in high energy density science. To reach a similar power output with collimated beams, a much greater beam diameter and a correspondingly more powerful seed pulse would be required.

A further advantage of this scheme over the collimated case is that the pulse will never reach relativistic intensity. In the collimated case, the length of the amplifier is limited by de-tuning due to the relativistic electron non-linearity[30]. This can happen even before the pulse degrades in to transverse filaments[31, 32]. In the new geometry, this problem is eradicated and the length is only limited by competing plasma instabilities.

Particle in cell simulation. The diverging seed ionisation scheme may be investigated with the use of fully kinetic particle simulations that initialise perfect Gaussian laser pulses. Although, full three-dimensional (3D) simulations are currently infeasible, the steady-state behaviour is also observed in two-dimensional (2D) Cartesian simulations. This is provided that, as before, $\alpha_0 \propto 1/\sqrt{t - t_f}$ outside its Rayleigh range. The derivation proceeds as before, except a becomes $2a$.

The particle-in-cell code Osiris[33, 34] was used to model the amplification of a diverging seed pulse. To reduce computational expense, the simulation used a spatial domain that enclosed only the seed pulse and moved with it. The domain size was $125\lambda_0$ by $1000\lambda_0$ transversely, where λ_0 is the pump wavelength.

To model the seed ionisation scheme, a neutral hydrogen gas was initialised across the entire simulated volume. A field ionisation model was used to initialise the free electrons at the appropriate time within the simulation. The electrons were
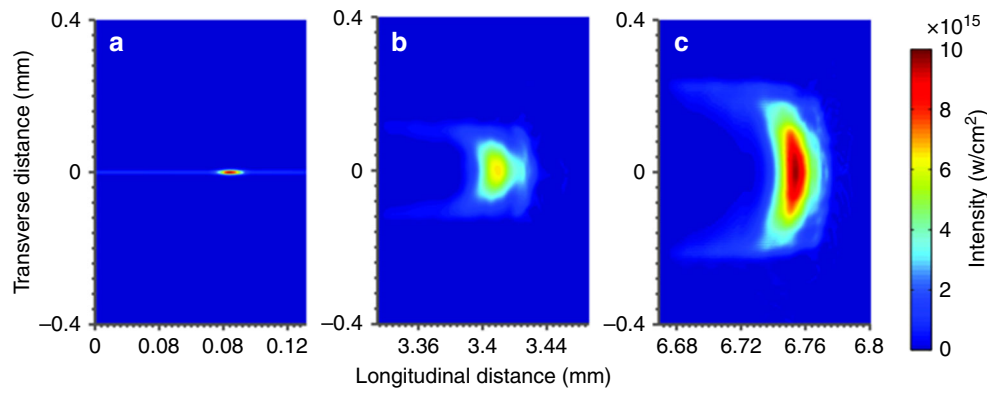
Fig. 3 Results of the two-dimensional particle-in-cell simulation. The intensity envelope of the diverging amplified pulse is shown at three time-steps in the simulation, at **a** 0 ps, **b** 11.2 ps and **c** 22.4 ps. The plasma was uniform with density 10^{19} cm^{-3} and the pump amplitude (visible on this colour scale only at the first time-step) decreased $a_0 \propto 1/\sqrt{t - t_f}$. The pulse propagates towards the right and it has been smoothed on a wavelength scale using a Gaussian filter
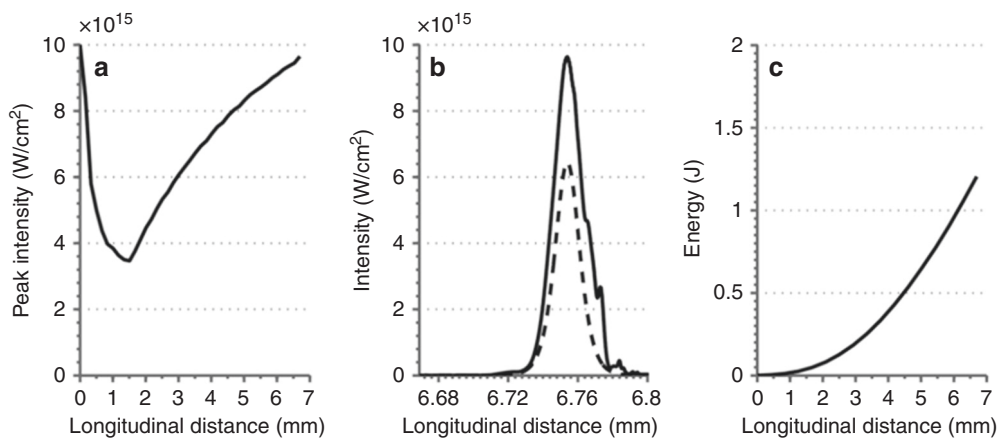
Fig. 4 Results of the two-dimensional particle-in-cell simulation. **a** The peak intensity of the amplified pulse, as it develops over the 6.7 mm propagation, starting at the focus. **b** A line-out (solid line) along the x axis of the final intensity envelope after 22.4 ps, given in Fig. 3c. The prediction of Eq. (15) is also shown with the dashed line. **c** The development of the energy of the amplified pulse. This was found from the two-dimensional data by assuming azimuthal symmetry

initialised with temperature 50 eV and uniform density 10^{19} cm^{-3}. The laser pulses were initialised as ideal Gaussian beams. The long-pump pulse had a constant wavelength 1.054 μm and on-axis amplitude that decreased as $a_0 \propto 1/\sqrt{t - t_f}$ outside of the Rayleigh range, such that $a = (t - t_f)a_0^2\sqrt{\omega_0\omega_p/8} = 0.08$. The focal beam waist was 6 μm.

The seed pulse was initialised at its focus, exactly counter-propagating with the pump pulse. The focal position and beam waist were the same as for the pump. The central wavelength was 1.18 μm, its peak amplitude was $a_1 = 0.1$, its peak intensity was 10^{16} W cm^{-2}, its duration was 50 fs and, extrapolated azimuthally, its energy was 0.3 mJ. The simulation followed the amplification and divergence of the short seed pulse for 22.4 ps (a propagation distance of 6.7 mm). The seed started close to the non-linear stage.

The development of the seed pulse intensity envelope is shown over three time-steps in Fig. 3. The pulse starts at its focus, then amplifies as it diverges. Because its amplitude decreases, the long-pump pulse is only visible on the colour scale in the first time-step.

Since the pump pulse intensity is higher on-axis, the pulse duration is slightly shorter in the centre. This leads to some transverse gain narrowing, where the focal angle of the amplified pulse is reduced somewhat. This effect could be minimised by

using a pump with a flat-top, rather than Gaussian transverse profile. There are some filament structures that permeate through the ionisation front ahead of the amplified pulse, although their growth saturates.

The development of the peak intensity over time is shown in Fig. 4a. The pulse initially drops in intensity as it diverges, then increases again as the Raman scatter converges to the asymptotic constant intensity solution, as predicted by Eq. (15). The peak intensity should eventually converge to a constant value, although the simulation did not continue long enough to observe this.

To assess the effect of ionisation on the final pulse wave-front, the phase of the pulse was found as a function of radial distance. It was found to deviate from a parabolic shape by <0.1 radians across the transverse width of the pulse. The corresponding radius of wave-front curvature was 6.2 mm, similar to the expected curvature of 6.7 mm for a Gaussian pulse in vacuum.

Figure 4b shows a line-out of the pulse envelope along the x axis, at the final time-step after 22.4 ps. As predicted, there are no secondary trailing peaks. Although, suppression of these peaks is also possible when the pump exceeds the threshold wave-breaking intensity[35–39], here this was only true for the first 20% of the propagation. We therefore attribute the suppression to the divergence of the pulse, rather than premature breaking of the plasma wave.

Also plotted with a dashed line in Fig. 4b is the prediction of Eq. (15). Since the simulation used a 2D geometry, the predicted convergent pulse amplitude is twice that of the 3D derivation. This explains why the intensity of the simulated pulse exceeds the 3D prediction. However, the shape of the temporal envelope is accurately reproduced.

In Fig. 4c, the energy of the amplified pulse is plotted as a function of the propagation distance. This was calculated by assuming azimuthal symmetry about the x axis and integrating the intensity profile. Although the intensity is approximately constant, the energy of the pulse increases by a factor of more than 4000. The overall pump to seed energy efficiency was 59%. This value is very high because the amplifier started in the non-linear stage from the beginning and the pump pulse was predominantly below the threshold wave-breaking intensity.

Discussion

Seed pulses in typical Raman amplifier experiments are not intense enough to reach the non-linear stage from the start, so there must first be a long stretch of the amplifier in the low efficiency linear stage. This lowers the overall efficiency. We propose that this stage can be avoided by starting the amplifier at the focus, maximising the effectiveness of the seed. Although some previous studies have used small spot sizes in plasma wave-guides[40, 41], the allowable pump energy is then constrained by the small plasma volume. The new diverging geometry increases the allowable pump energy while retaining the minimal seed pulse requirements.

We have shown that if the pump pulse power increases linearly with time, the seed has constant intensity as it amplifies and diverges. In fact, the usual trailing secondary spikes of the standard solution are eliminated, concentrating more energy in the front-most spike. The geometry also enables easy use of the seed ionisation scheme, which has many further advantages. Furthermore, unlike the collimated case, the seed never reaches relativistic intensity and so de-tuning due to the relativistic electron non-linearity is avoided.

The geometry offers a route to scale up the amplifiers to use nanosecond long-pump pulses, as discussed in ref.[26]. The design could utilise a multi-kilojoule pump pulse with a sub-millijoule seed to reach unprecedented pulse powers. The growth of a 0.3 mJ seed has been simulated to over 1.2 J, with the only eventual limitation set by competing instabilities such as Raman forward scattering and filamentation of the amplified pulse.

Methods

Computer simulation algorithm. The simulation used the particle-in-cell code Osiris, version 2. The grid was Cartesian in two dimensions. The main loop of the algorithm repeats a process that advances the plasma by a finite time-step. First, it interpolates the charge and current densities of a large number of particles to a spatial grid. The grid resolves the Debye length, along with the electromagnetic and plasma wavelengths. The electric and magnetic fields are known on the grid and are advanced in time using the Maxwell equations. The fields are interpolated to the position of each particle and used to update their momentum and position.

As such, the development of the pulse is found directly from the Maxwell equations and all particle trapping effects are modelled in the simulation[42]. Collisional damping is not modelled in the simulation, however the pump will be largely unaffected because the plasma is only ionised at the position of the short seed pulse. The inverse collisional damping rate is much longer than the seed pulse, so inclusion of collisional damping should barely change the interaction. The domain moved with the amplified pulse at a velocity $0.994c$, by initialising new cells at the front of the domain and deleting those at the rear. The pump pulse was also initialised at the leading edge. The laser pulses were initialised as perfect Gaussian beams.

Analysis of the computer simulation. Initially the pump pulse ionised the plasma, but after 1 mm the pump pulse beam waist was wider and it was below the ionisation intensity. From here onwards, the plasma was ionised by the seed pulse. Plasma instabilities of the pump pulse across the 1 mm region near the focus were

not modelled. If the pump pulse is excessively degraded by instabilities in this region, it could be reduced in size by increasing the focal angle.

The grid resolution was $\lambda_0/60$ by $\lambda_0/2$ transversely. There were 32 electron particles per cell and the ions were held static to reduce computational costs. The simulation used open boundary conditions and cubic particle interpolation. The pulses had aligned linear polarisation.

The pulse envelope was extracted by saving the electromagnetic energy density in each cell at intervals of 280 fs, then smoothing the data on a wavelength scale using a 2D Gaussian filter. The simulated energy of the pulse was extracted by taking the data on only one side of the x axis, assuming the pulse is axially symmetric, then integrating radially and longitudinally using the Jacobian for cylindrical coordinates to obtain the volumetric integral. The total energy efficiency was found by integrating the final seed pulse energy density in two dimensions to obtain a quantity with units J cm^{-1}. The equivalent figure for the pump was found by integrating the unperturbed pump energy density across the simulation domain, then multiplying by the ratio of the pump pulse length to the length of the simulation domain, since the simulated pump power was constant. The overall simulated efficiency is the ratio of these values.

References

1. Strickland, D. & Mourou, G. Compression of amplified chirped optical pulses. *Opt. Commun.* **55**, 447–449 (1985).
2. Di Piazza, A., Müller, C., Hatsagortsyan, K. & Keitel, C. Extremely high-intensity laser interactions with fundamental quantum systems. *Rev. Mod. Phys.* **84**, 1177–1228 (2012).
3. King, B., Di Piazza, A. & Keitel, C. H. Double-slit vacuum polarization effects in ultraintense laser fields. *Phys. Rev. A* **82**, 032114 (2010).
4. Ridgers, C. et al. Dense electron-positron plasmas and ultraintense γ rays from laser-irradiated solids. *Phys. Rev. Lett.* **108**, 165006 (2012).
5. Bjørnholm, S. & Lynn, J. The double-humped fission barrier. *Rev. Mod. Phys.* **52**, 725–931 (1980).
6. Tabak, M. et al. Ignition and high gain with ultrapowerful lasers. *Phys. Plasmas* **1**, 1626–1634 (1994).
7. Roth, M. et al. Fast ignition by intense laser-accelerated proton beams. *Phys. Rev. Lett.* **86**, 436–439 (2001).
8. Ratan, N. et al. Dense plasma heating by crossing relativistic electron beams. *Phys. Rev. E* **95**, 013211 (2017).
9. Ceurvorst, L. et al. Mitigating the hosing instability in relativistic laser-plasma interactions. *New. J. Phys.* **18**, 053023 (2016).
10. Norreys, P. Auxiliary heating of inertial confinement fusion targets. In *APS Meeting Abstracts* Bulletin of the American Physical Society 59 (2014).
11. Malkin, V., Shvets, G. & Fisch, N. Fast compression of laser beams to highly overcritical powers. *Phys. Rev. Lett.* **82**, 4448–4451 (1999).
12. Milroy, R., Capjack, C. & James, C. Plasma laser pulse amplifier using induced Raman or Brillouin processes. *Phys. Fluids* **22**, 1922–1931 (1979).
13. Trines, R. et al. Simulations of efficient raman amplification into the multipetawatt regime. *Nat. Phys.* **7**, 87–92 (2011).
14. Sadler, J. D. et al. Robustness of raman plasma amplifiers and their potential for attosecond pulse generation. *High Energy Density Phys.* **23**, 212–216 (2017).
15. Sadler, J. D. et al. Optimization of plasma amplifiers. *Phys. Rev. E* **95**, 053211 (2017).
16. Clark, D. S. & Fisch, N. J. Operating regime for a backward raman laser amplifier in preformed plasma. *Phys. Plasmas* **10**, 3363–3370 (2003).
17. Clark, D. S. & Fisch, N. J. Particle-in-cell simulations of raman laser amplification in preformed plasmas. *Phys. Plasmas* **10**, 4848–4855 (2003).
18. Ping, Y., Geltner, I., Fisch, N., Shvets, G. & Suckewer, S. Demonstration of ultrashort laser pulse amplification in plasmas by a counterpropagating pumping beam. *Phys. Rev. E* **62**, R4532–R4535 (2000).
19. Ren, J. et al. A compact double-pass raman backscattering amplifier/compressor. *Phys. Plasmas* **15**, 056702 (2008).
20. Malkin, V. & Fisch, N. Backward raman amplification of ionizing laser pulses. *Phys. Plasmas* **8**, 4698–4699 (2001).
21. Clark, D. S. & Fisch, N. J. Regime for a self-ionizing raman laser amplifier. *Phys. Plasmas* **9**, 2772–2780 (2002).
22. Clark, D. S. & Fisch, N. J. Simulations of raman laser amplification in ionizing plasmas. *Phys. Plasmas* **10**, 4837–4847 (2003).

23. Doumy, G. et al. Complete characterization of a plasma mirror for the production of high-contrast ultraintense laser pulses. *Phys. Rev. E* **69**, 026402 (2004).

24. Dromey, B., Kar, S. & Zepf, M. The plasma mirror—a subpicosecond optical switch for ultrahigh power lasers. *Rev. Sci. Instrum.* **75**, 645–649 (2004).

25. Fraiman, G. M., Yampolsky, N. A., Malkin, V. M. & Fisch, N. J. Robustness of laser phase fronts in backward raman amplifiers. *Phys. Plasmas* **9**, 3617–3624 (2002).

26. Trines, R. et al. Production of picosecond, kilojoule, and petawatt laser pulses via raman amplification of nanosecond pulses. *Phys. Rev. Lett.* **107**, 105002 (2011).

27. Dodin, I., Fraiman, G., Malkin, V. & Fisch, N. Amplification of short laser pulses by raman backscattering in capillary plasmas. *J. Exp. Theor. Phys.* **95**, 625–638 (2002).

28. Haynam, C. et al. National ignition facility laser performance status. *Appl. Opt.* **46**, 3276–3303 (2007).

29. Toroker, Z., Malkin, V. M. & Fisch, N. J. Seed laser chirping for enhanced backward Raman amplification in plasmas. *Phys. Rev. Lett.* **109**, 085003 (2012).

30. Malkin, V., Toroker, Z. & Fisch, N. Laser duration and intensity limits in plasma backward raman amplifiers. *Phys. Plasmas* **19**, 023109 (2012).

31. Malkin, V., Toroker, Z. & Fisch, N. Saturation of the leading spike growth in backward raman amplifiers. *Phys. Plasmas* **21**, 093112 (2014).

32. Yampolsky, N. A. & Fisch, N. J. Limiting effects on laser compression by resonant backward raman scattering in modern experiments. *Phys. Plasmas* **18**, 056711 (2011).

33. Fonseca, R. et al. Osiris: A three-dimensional, fully relativistic particle in cell code for modeling plasma based accelerators. *Lect. Notes Comput. Sci.* **2331**, 342–351 (2002).

34. Fonseca, R. A. et al. Exploiting multi-scale parallelism for large scale numerical modelling of laser wakefield accelerators. *Plasma Phys. Control. Fusion* **55**, 124011 (2013).

35. Coffey, T. Breaking of large amplitude plasma oscillations. *Phys. Fluids* **14**, 1402–1406 (1971).

36. Toroker, Z., Malkin, V. & Fisch, N. Backward raman amplification in the langmuir wavebreaking regime. *Phys. Plasmas* **21**, 113110 (2014).

37. Edwards, M. R., Toroker, Z., Mikhailova, J. M. & Fisch, N. J. The efficiency of raman amplification in the wavebreaking regime. *Phys. Plasmas* **22**, 074501 (2015).

38. Farmer, J., Ersfeld, B. & Jaroszynski, D. Raman amplification in plasma: wavebreaking and heating effects. *Phys. Plasmas* **17**, 113301 (2010).

39. Yampolsky, N. et al. Demonstration of detuning and wavebreaking effects on raman amplification efficiency in plasma. *Phys. Plasmas* **15**, 113104 (2008).

40. Pai, C. H. et al. Backward raman amplification in a plasma waveguide. *Phys. Rev. Lett.* **101**, 065005 (2008).

41. Vieux, G. et al. Chirped pulse raman amplification in plasma. *New. J. Phys.* **13**, 063042 (2011).

42. Hur, M. S., Lindberg, R., Charman, A., Wurtele, J. & Suk, H. Electron kinetic effects on raman backscatter in plasmas. *Phys. Rev. Lett.* **95**, 115003 (2005).

Author contributions

J.D.S. undertook the mathematical study and simulation of the new scheme and wrote the paper. L.O.S. and R.A.F. contributed to the simulation code. K.G., M.F.K., A.S., R.A., M.W.M., B.S., R.H.W.W. and R.B. contributed to discussion, corrections and development of the idea. R.M.G.M.T. and P.A.N. supervised the research.

Additional information

Competing Interests: The authors declare no competing interests.